Geophysical Research Letters

RESEARCH LETTER
10.1029/2022GL102263

Do the Throat Auroras Create Polar Cap Patches?

Duan Zhang[1], Qing-He Zhang[1], Kjellmar Oksavik[2,3], Tong Xu[4], Zan-Yang Xing[1], L. R. Lyons[5], De-Sheng Han[6], Hong-Bo Zhang[4], Yu-Zhang Ma[1], Ze-Jun Hu[7], Jian-Jun Liu[7], Yong Wang[1], and Xiang-Yu Wang[1]

[1]Shandong Provincial Key Laboratory of Optical Astronomy and Solar-Terrestrial Environment, Institute of Space Sciences, Shandong University, Weihai, China, [2]Birkeland Centre for Space Sciences, Department of Physics and Technology, University of Bergen, Bergen, Norway, [3]Arctic Geophysics, University Centre in Svalbard, Longyearbyen, Norway, [4]National Key Laboratory of Electromagnetic Environment, China Research Institute of Radiowave Propagation, Qingdao, China, [5]Department of Atmospheric and Oceanic Sciences, University of California, Los Angeles, CA, USA, [6]State Key Laboratory of Marine Geology, School of Ocean and Earth Science, Tongji University, Shanghai, China, [7]Polar Research Institute of China, Shanghai, China

Key Points:

- The formation of throat auroras and polar cap patches is studied with multiple instruments in space and on ground
- Both throat auroras and polar cap patches are closely linked as they move poleward
- The formation of throat auroras and patches is associated with magnetic reconnection for dominant radial interplanetary magnetic field

Supporting Information:

Supporting Information may be found in the online version of this article.

Correspondence to:

Q.-H. Zhang,
zhangqinghe@sdu.edu.cn

Citation:

Zhang, D., Zhang, Q.-H., Oksavik, K., Xu, T., Xing, Z.-Y., Lyons, L. R., et al. (2023). Do the throat auroras create polar cap patches? *Geophysical Research Letters*, *50*, e2022GL102263. https://doi.org/10.1029/2022GL102263

Received 23 NOV 2022
Accepted 24 MAR 2023

Abstract Throat auroras and polar cap patches are common phenomena in the polar ionosphere resulting from magnetosphere-ionosphere coupling. A campaign was organized, with all-sky imagers at Yellow River Station, the European Incoherent Scatter Svalbard Radar, and coordinated low-altitude spacecraft observations. During periods of radial interplanetary magnetic field (IMF), observations showed that, as poleward moving throat auroras faded around the polar cap boundary, they linked to poleward moving ionization patches. The throat auroras were produced by soft-electron precipitation associated with dayside magnetic reconnection. The red line emission intensity of throat auroras was correlated with dayside reconnection events. Dense plasma from lower latitudes was transported poleward via enhanced convection in the throat auroras to form patches. This is a potentially new formation mechanism for patches associated with throat auroras and magnetic reconnection for radial IMF. Moreover, the patches move anti-sunward due to the $E \times B$ drift.

Plain Language Summary The polar ionosphere is a key region in the solar wind-magnetosphere-ionosphere coupling processes. The throat auroras and polar cap patches are important phenomenon in the polar ionosphere, and are associated with magnetopause dynamic processes. To clarify the relationship between throat auroras and patches, we organized a campaign of multiple instruments observations of Yellow River Station all-sky imagers, European Incoherent Scatter Svalbard Radar, and low-altitude spacecraft observations. We found that the throat auroras and patches were closely linked as they move poleward. The throat auroras were produced by soft-electron precipitation associated with dayside magnetic reconnection for radial interplanetary magnetic field (IMF). We proposed a potentially new formation mechanism for patches from throat auroras under IMF B_x-dominant that high density plasma from lower latitudes was transported poleward via enhanced convection in the throat auroras to form patches. Moreover, the patches moved anti-sunward due to the $E \times B$ plasma drift.

1. Introduction

Throat auroras and polar cap patches are common phenomena in the polar ionosphere resulting from solar wind-magnetosphere-ionosphere coupling. The throat aurora is a discrete aurora that is associated with localized magnetopause indentations (Han, 2019). It is usually located equatorward of the cusp aurora oval near magnetic noon, oriented in the south-north direction (Han et al., 2015) and is more frequently observed under radial interplanetary magnetic field (IMF, Bx-dominated conditions) (e.g., Han et al., 2017; Rodriguez et al., 2012). Han et al. (2016) indicated that throat aurora is an ionospheric feature in which magnetosheath particles enter the magnetosphere along open magnetic field lines, based on data from ground-based all-sky imagers (ASIs) and Magnetospheric Multiscale (MMS) satellites. Throat auroras are also observed to be accompanied by Joule heating and ion upflows, based on data from a European Incoherent Scatter (EISCAT) radar experiment (Han et al., 2019), which supports throat aurora being associated with magnetopause reconnection.

The polar cap patch is another common phenomenon in the dayside ionosphere polar regions. It is also associated with transient dayside reconnection (e.g., Carlson et al., 2004; Lockwood & Carlson, 1992; Zhang et al., 2011, 2013). A patch is an island of high-density F region ionospheric plasma with a typical size of

~100–1,000 km (e.g., Carlson, 2012; Coley & Heelis, 1995) that is more frequently observed under southward IMF conditions (e.g., Jin et al., 2018; Zhang et al., 2020). The patch forms near the dayside dynamic cusp, and it has been shown to be related to dayside aurora structures like the poleward moving auroral form (PMAF) (e.g., Nishimura et al., 2014; Lorentzen et al., 2010). Lorentzen et al. (2010) introduced a model to explain that there remains a region of enhanced plasma density and emission caused by previous particle precipitation when the PMAF fades (Hosokawa et al., 2016). The enhanced plasma is lifted vertically upwards in the F region due to the field-aligned current and the enhanced Pedersen conductivity. Zhang et al. (2011) used the poleward moving radar aurora forms (PMRAFs) to explain how patch material is generated by photoionization at subauroral latitudes and structured by magnetopause reconnection. Thus, the throat aurora, as a prominent auroral structure at subauroral latitudes, may also play a similar key role in polar cap patch creation, which needs to be investigated.

In this study, a multi-instrument observation campaign was carried out in the polar ionosphere in December 2018, with three ASIs at Yellow River Station (YRS), two antenna beams of the EISCAT Svalbard Radar (ESR), and coordinated in situ observations from the Defense Meteorological Satellite Program (DMSP) and Swarm satellites to reveal the connection between throat aurora and patch formation. The YRS ASIs successfully observed the sequential motion of throat auroras and patches from low latitudes to high latitudes on 6 December 2018. The ESR, DMSP, and Swarm added additional context. Moreover, in this paper we propose a new formation mechanism for polar cap patches associated with throat auroras and magnetic reconnection for radial IMF.

2. Data Sources

An optical observation system (Hu et al., 2009) was installed at the YRS at Ny-Ålesund (78.92°N, 11.93°E) in Svalbard in 2003. The three ASIs simultaneously observe three different wavelengths at 427.8, 557.7, and 630.0 nm, and were projected to magnetic latitudes using emission heights of 120, 150, and 220 km, respectively. The ASI at 557.7 nm observes the aurora associated with energetic particle precipitation, and the 630.0 nm detects the auroras formed by soft-electron precipitation, such as throat auroras. The time resolution of images is 10 s.

The ESR at Longyearbyen (78.09°N, 16.02°E) consists of a 32 m steerable parabolic dish antenna and a 42 m field-aligned (81.6° elevation) antenna. The ESR offers electron density (Ne), ion and electron temperatures (Ti and Te), and line-of-sight ion velocity (Vi). In this study, the 32 m antenna was fixed at an elevation of 30° and an azimuth of 0°, which points to the geographic north pole.

The DMSP satellites are polar-orbiting spacecrafts in about 835–860 km altitude with 101 min orbital period. The Precipitating Electron and Ion Spectrometer (SSJ/5) (Hardy et al., 2008) observes precipitating electrons and ions in the range of 32 eV to 30 keV. The Special Sensor Ultraviolet Spectrographic (SUSSI) instrument (Paxton et al., 1992) measures ultraviolet (UV) emissions in five different wavelengths. We use the Lyman-Birge-Hopfield short (LBHS) band (~140–150 nm) observation, whose intensity is associated with the auroral energy flux (Knight et al., 2008).

The Swarm satellites are near polar-orbiting spacecrafts with 93 min orbital period, consisting of three satellites. The Swarm-A and Swarm-C fly side by side at about 460 km altitude with an inclination of 87.4°, and the Swarm-B fiy about 520 km with an inclination of 87.8°. We use the Langmuir probe (LP) electron density data with 0.5 s data cadence rate observed by Swarm-A and Swarm-C (Buchert et al., 2015).

The solar wind and IMF data from 1-min high resolution OMNI database. We apply a 7-min time delay to these data to account for the response time of the solar wind from the subsolar magnetopause to the dayside ionosphere. It is estimated to be the sum of 5 min for traversing from the bow shock to the magnetopause and 2 min for traversing from the magnetopause to the ionosphere (e.g., Hu et al., 2017; Liou et al., 1998).

3. Observations Results

The YRS ASIs observed a close link between throat auroras and patches on 6 December 2018. There were three throat auroras from 0800 to 0840 universal time (UT) (~1100–1140 magnetic local time (MLT)). Figure 1a shows three bright throat aurora arcs equatorward of the dayside auroral oval at about 11 MLT (dashed orange box, magnified in the lower right corner, and labeled A-C) from DMSP F17 SUSSI data plotted in MLT—magnetic latitude (MLAT) coordinates. The DMSP F17 trajectory, Swarm A and C trajectories, field-of-view of the 630.0 nm ASI at YRS, and the ESR 32 and 42 m, are indicated by a dashed white line, magenta circle,

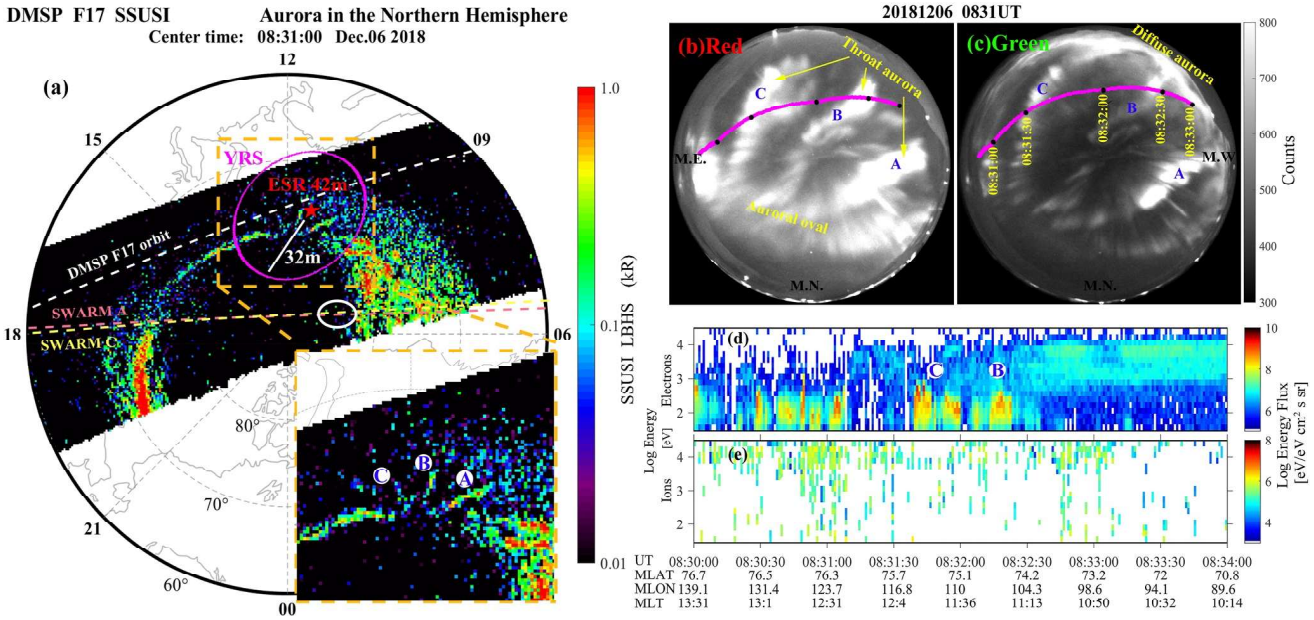

Figure 1. In situ plasma and aurora observations in the Northern Hemisphere on 6 December 2018. (a) The Defense Meteorological Satellite Program (DMSP) F17 Special Sensor Ultraviolet Spectrographic observation in the Lyman-Birge-Hopfield short (LBHS) band and DMSP F17 trajectory (dashed white line), Swarm A and C trajectories (dashed pink and yellow lines), the field-of-view of the Yellow River Station (YRS) 630.0 nm all-sky imager (magenta circle), the ESR 32m (solid white line) and 42m (red star) plotted in magnetic local time-magnetic latitude coordinates. The white circle highlights the location of enhanced electron density observed by Swarm A and C. (b andc) The snapshots of the red and green line auroras observed at 0831 UT (magnetic north is at the bottom, magnetic east to the left), and the DMSP F17 trajectory across the YRS field-of-view at ~0831–0833 UT (magenta lines). (d–e) The electron and ion energy flux observations from DMSP F17.

solid white line, and red star, respectively. Figures 1b and 1c show snapshots of the YRS ASIs red and green line auroral observations at 0831 UT matching the center time of SUSSI observation, and the DMSP F17 trajectory is shown as magenta lines. The particle observations for electrons and ions from DMSP F17 are shown in Figures 1d and 1e. The equatorward of the throat auroras appear as stripy diffuse auroras in green line (e.g., Han et al., 2015). The throat auroras B and C are associated with soft-electron precipitation, which is consistent with the previous studies. The full evolution of the three throat auroras and patches is shown in Movie S1. There are many fine structures in the throat auroras from low to high latitudes.

Figures 2a and 2b show the IMF B_x, B_y, B_z in Geocentric Solar Magnetic (GSM) coordinates, and the solar wind velocity (V_{sw}) and density (N_p), from the OMNI database with a 7-min time delay from 0800 to 0840 UT. During this period, IMF was mainly radial and dominated by negative B_x component. B_y remained positive throughout. B_z was initially negative, and it turned positive at ~0815 UT, and then it became negative again at ~0818 UT. The radial IMF with negative B_x is very common for the generation of throat auroras (Han et al., 2019). The V_{sw} varied between 380 and 390 km/s, and the N_p varied between 2.5 and 3 cm^{-3}. To parameterize the solar wind driving, we calculate the dayside magnetopause reconnection rate (coupling function) during the observation period in Figure 2c via the parametric function given by Milan et al. (2012):

$$\varnothing_D = 3.2 \times 10^5 V_{sw}^{4/3} B_{yz} \sin^{9/2}\left|\frac{1}{2}\theta\right|$$

In this function, $\theta = \tan^{-1}(B_y, B_z)$ is the IMF clock angle, and $B_{yz} = \sqrt{B_y^2 + B_z^2}$ is the magnitude of the transverse component of the IMF. Figure 2d shows the throat auroras mean intensity at 630.0 nm. The calculation process is as follows: first, the throat auroras are almost in the range of approximately 74–78° MLAT which is shown in the ASIs. Then, we selected the ASIs data in the range of 74–76.5° MLAT to eliminate the influence of the dayside aurora oval (~76.5–78° MLAT) emission intensity on the calculation of the throat aurora emission intensity. Finally, we calculated the mean intensity of all pixels greater than 500 counts (choosing 450, 500, 550, or 600 counts give similar results) to represent the throat aurora mean intensity. Note that the last step is for eliminating sky-noise and background effects. Figure 2e shows that the keogram of the YRS ASIs auroral emission intensity along the magnetic meridian. The emission intensity first decreased slowly and then increased

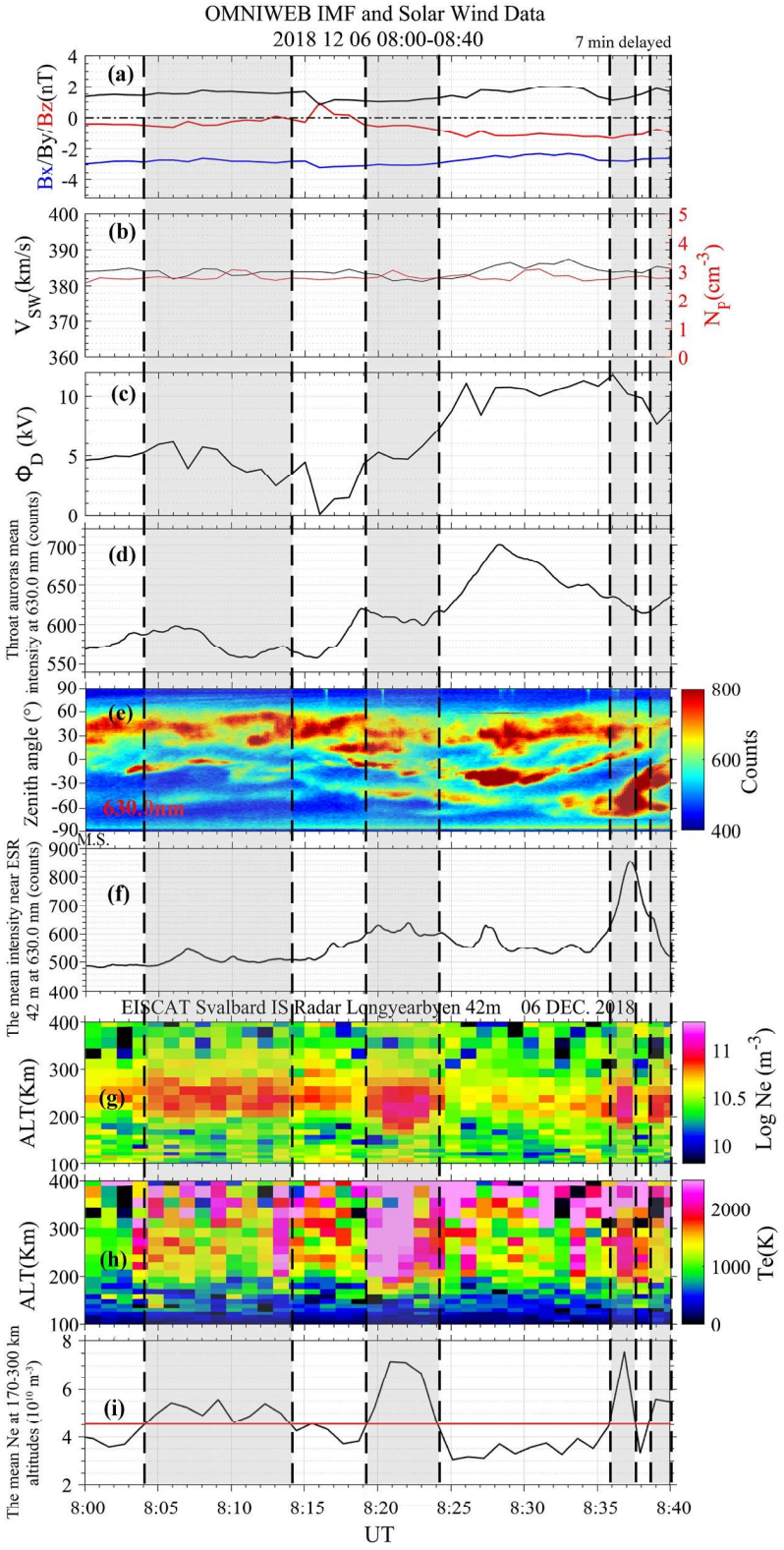
OMNIWEB IMF and Solar Wind Data
2018 12 06 08:00-08:40
7 min delayed
(a)
Bx/By/Bz(nT)
(b)
V_{SW}(km/s)
N_p(cm^{-3})
(c)
Φ_D (kV)
(d)
Throat auroras mean intensiy at 630.0 nm (counts)
(e)
Zenith angle (°)
630.0nm
M.S.
Counts
(f)
The mean intensity near ESR 42 m at 630.0 nm (counts)
EISCAT Svalbard IS Radar Longyearbyen 42m 06 DEC. 2018
(g)
ALT(Km)
Log Ne (m^{-3})
(h)
ALT(Km)
Te(K)
(i)
The mean Ne at 170-300 km altitudes (10^{10} m^{-3})
8:00
8:05
8:10
8:15
8:20
8:25
8:30
8:35
8:40
UT

Figure 2.

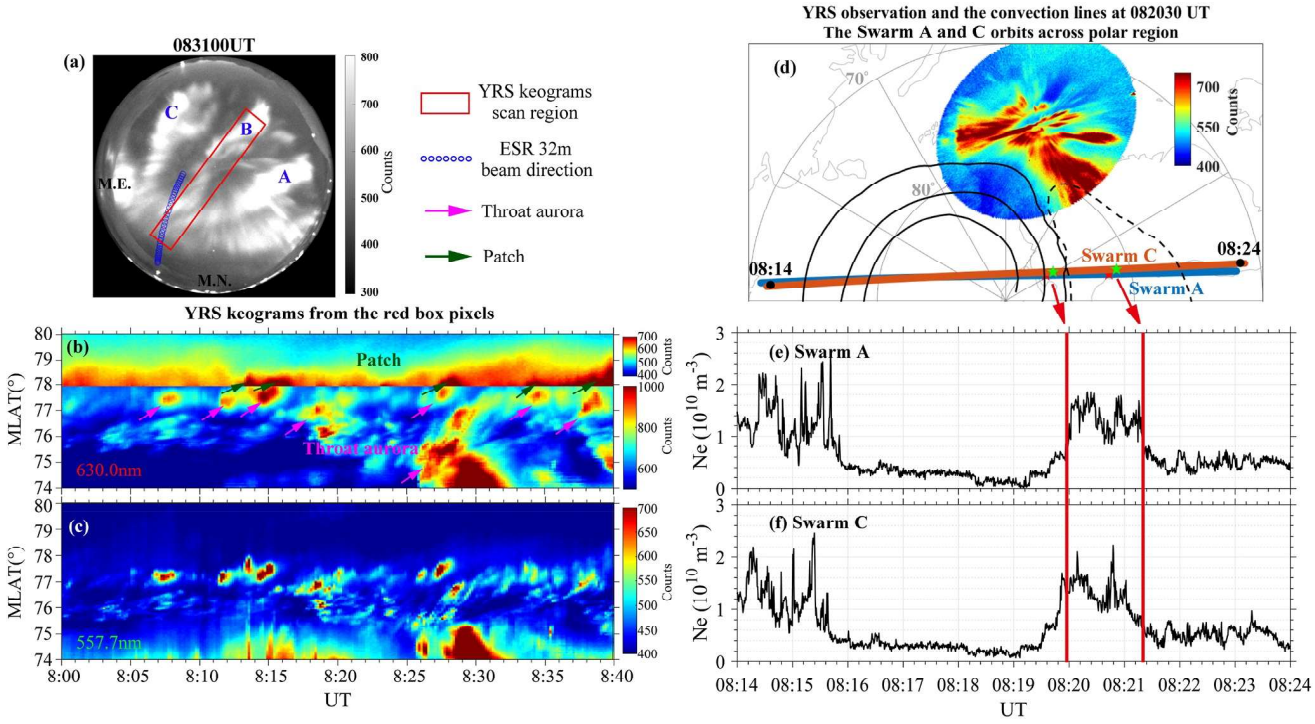

Figure 3. (a) Image from the 630.0 nm Yellow River Station (YRS) all-sky imager at 0831 UT. The blue markers highlight the antenna beam direction of the ESR 32 m. The red box marks the area that was used to produce the keograms. (b and c) Keograms of 630.0 and 557.7 nm emission intensities obtained in the red box in panel (a). The throat auroras and patches are highlighted by magenta and dark green arrows. Each bin is 0.05° magnetic latitude wide along the *y*-axis. (d) The YRS ASIs observation and the ionosphere convection pattern observed by SuperDARN at 082030 UT. The orbits of Swarm A and C are superimposed. (e and f) The electron density observations from Swarm A and C. The red lines highlight the electron density enhancement corresponding to the star marks on the Swarm orbits in panel (d).

rapidly after 0818 UT. Figure 2f shows the mean emission intensity at 630.0 nm near the location of the ESR 42m. Figures 2g and 2h display the field-aligned ESR 42 m antenna basic plasma parameters of electron density and temperatures. Figure 2i shows the mean electron density at 170–300 km in the ESR 42 m observations. The red line is the mean values during 0800–0840 UT. The observed throat auroras are highlighted by black vertical dashed lines and gray shading according to the regions which are higher than the red line in Figure 2i. High electron temperatures were observed in the throat auroras, which is indicative of electron precipitation. Note that high electron temperatures do not always correspond to throat auroras. Comparing Figures 2f and 2h, the emission intensity enhancements nearly coincide with electron temperatures enhancements.

Figure 3a shows the 630.0 nm YRS ASI observation at 0831 UT. The blue markers highlight the antenna beam direction of the ESR 32m. The red box marks the area that was used to produce the keograms in panels b and c. Two criteria were used to select the area of the keograms: (a) Cover the throat aurora for as much time as possible; (b) Overlap with the ESR 32m observation area for easier comparison. Figure 3b-3c show the resulting keograms of 630.0 and 557.7 nm emissions intensity. Each bin is 0.05° MLAT wide along the *y*-axis, and we have calculated the third quartile in each bin to exclude background emissions. Since the patches are much weaker in intensity than the throat auroras (Hosokawa et al., 2019), we changed the 630.0 nm colorbar between 78° and 80° MLAT (approximate location of patches). The throat auroras and patches are further highlighted by magenta and dark green arrows, respectively. The throat auroras in the keograms are mainly referred to as throat aurora B, and only the last one is referred to as throat aurora C. The throat auroras and patches move poleward. As the throat auroras fade, the patches appear further poleward (north of 78° MLAT) in Figure 3b. This provides observational support for a link between throat aurora and patches. Diffuse green auroras are sometimes observed at the equatorward

Figure 2. (a–b) interplanetary magnetic field $B_x/B_y/B_z$, solar wind velocity (V_{sw}) and density (N_p) from the OMNI database, (c) the dayside magnetopause reconnection rate, (d) the mean throat aurora intensity at 630.0 nm, and (e) a keogram of the Yellow River Station all-sky emission intensity along the magnetic meridian. (f) The mean emission intensity at 630.0 nm near the ESR 42 m beam. The ESR 42 m basic plasma parameters of (g) electron density, and (h) ion and electron temperatures. (i) The mean electron density at 170–300 km (black line) compared to the 0800–0840 UT average (red line). The observed throat auroras are highlighted by black vertical dashed lines and gray shading.

edge of throat auroras (Han et al., 2017). Please notice that the red box does not always cover the full extent of the throat aurora. The entire throat aurora entered the red box around 0824–0833 UT, and only the poleward portion of the throat aurora entered the red box at other times. Figure 3d shows the YRS ASIs observation and the ionosphere convection pattern observed by Super Dual Auroral Radar Network (SuperDARN) at 082030 UT. The trajectories of Swarm A and C during this time are superimposed. Figures 3e and 3f show the electron density observations from Swarm A and C. The red lines highlight the electron density enhancement corresponding to the star marks on the Swarm satellites trajectories. This suggests that patches may move poleward along the ionosphere convection streamlines. Combined with the DMSP SUSSI observations, the location of enhanced densities (white circle in Figure 1a) is in the polar cap. The electron densities return to much lower values when cross the dawnside auroral oval. That imply that any possible contribution from aurora particle precipitation is small.

Figures 4a–4d show (a) the electron density, (b–c) the ion and electron temperatures, and (d) the ion line-of-sight velocity observed by the ESR 32 m at a fixed elevation of 30° and azimuth of 0°. Positive velocities are away from the radar (i.e., poleward into the polar cap). The black lines highlight six patches (labeled I–VI) characterized by poleward motion (~200–500 m/s) and enhanced electron density. The dashed gray line in panel a marks the terminator location (solar zenith angle (SZA) ~107° = 90° + arccos (6,371/6,671)) along the geomagnetic meridian of Longyearbyen (~111°E) at 300 km. It suggests that the F-region ionosphere south of ~79° MLAT was illuminated. However, when the SZA is more than 90°, the sunlight will arrive from below, which means that the solar spectrum is subject to additional absorption as it passes through lower parts of the atmosphere towards Longyearbyen. This indicates that the solar extreme ultraviolet radiation (EUV) production of high-density plasma is less likely as a plasma source of patches. The electron temperature of the patches "III" and "V" is mainly similar or slightly lower than that of the surroundings, which is characteristic of cold patches (e.g., Ma et al., 2018; Zhang et al., 2017, 2021, 2022). The other patches are more likely to be a mix of cold and hot patches. Figure 4c suggests that there is enhanced Joule heating associated with these patches. Figures 4e and 4f show the YRS red line ASI in MLT-MLAT coordinates, with ESR 32 m electron density observations overlaid according to the color scale. Some fine structures in the throat auroras are highlighted by the black arrows with white borders. The magenta circles highlight the patch "IV." The electron density observed by ESR 32 m was clearly enhanced when one fine structure (a bright aurora bin highlighted by the black arrow close to the line-of-sight of ESR 32 m) in the throat aurora reaches the line-of-sight. The throat auroras with many fine structures and patches move poleward, and patches are seen to appear at the most poleward location of throat auroras. An animation of 630.0 nm ASI at YRS and ESR 32 m observations is shown in Movie S2, which shows the complete evolution of throat auroras into patches. The other patches and throat auroras show similar relationships as the patch "IV."

4. Discussion

Based on data from multiple instruments (YRS ASIs, ESR, DMSP, and Swarm), this study has linked throat auroras and patch formation. Figures 1b–1d show that DMSP F17 sequentially traversed the throat auroras "C" and "B" at ~083130–083230 UT and observed enhanced soft-electron (<1 keV) precipitation. The anti-sunward flow bursts often occur on the western edge of throat auroras, which means that the throat auroras are associated with clockwise flow vorticity (hence upward field-aligned currents (FACs)) (e.g., Han et al., 2019; Southwood, 1987), consistent with enhanced electron precipitation. The soft-electron precipitation is one key energy source of ion upflows in the dayside ionosphere (e.g., Moen et al., 2004; Ogawa et al., 2003), suggesting frequent ion upflows over throat auroras.

As the dayside magnetopause connection rate changed, Figure 2 shows that the red line emission intensity of the throat auroras first decreased slowly, and then increased rapidly after 0818 UT. This supports the point that throat auroras are associated with magnetopause reconnection (Han, 2019), and are closely linked to an active coupling process of the solar-terrestrial system. The solar wind and IMF conditions were relatively stable, allowing the throat auroras to be present for tens of minutes.

Figure 3b and Movies S1 and S2 show the poleward motion of throat auroras and evolution into polar cap patches. The poleward motion suggests that they are associated with dayside magnetopause reconnection (Han et al., 2019). When the throat auroras move poleward into the polar cap, patches will be generated that are associated with transient magnetic reconnection. Movie S1 and Figures 4e and 4f indicate the progression of many fine structures in the throat auroras from lower to higher latitudes. As they move, high-density plasma is pushed poleward from subauroral latitudes in the form of cold patches in the lack of a heat source. The soft

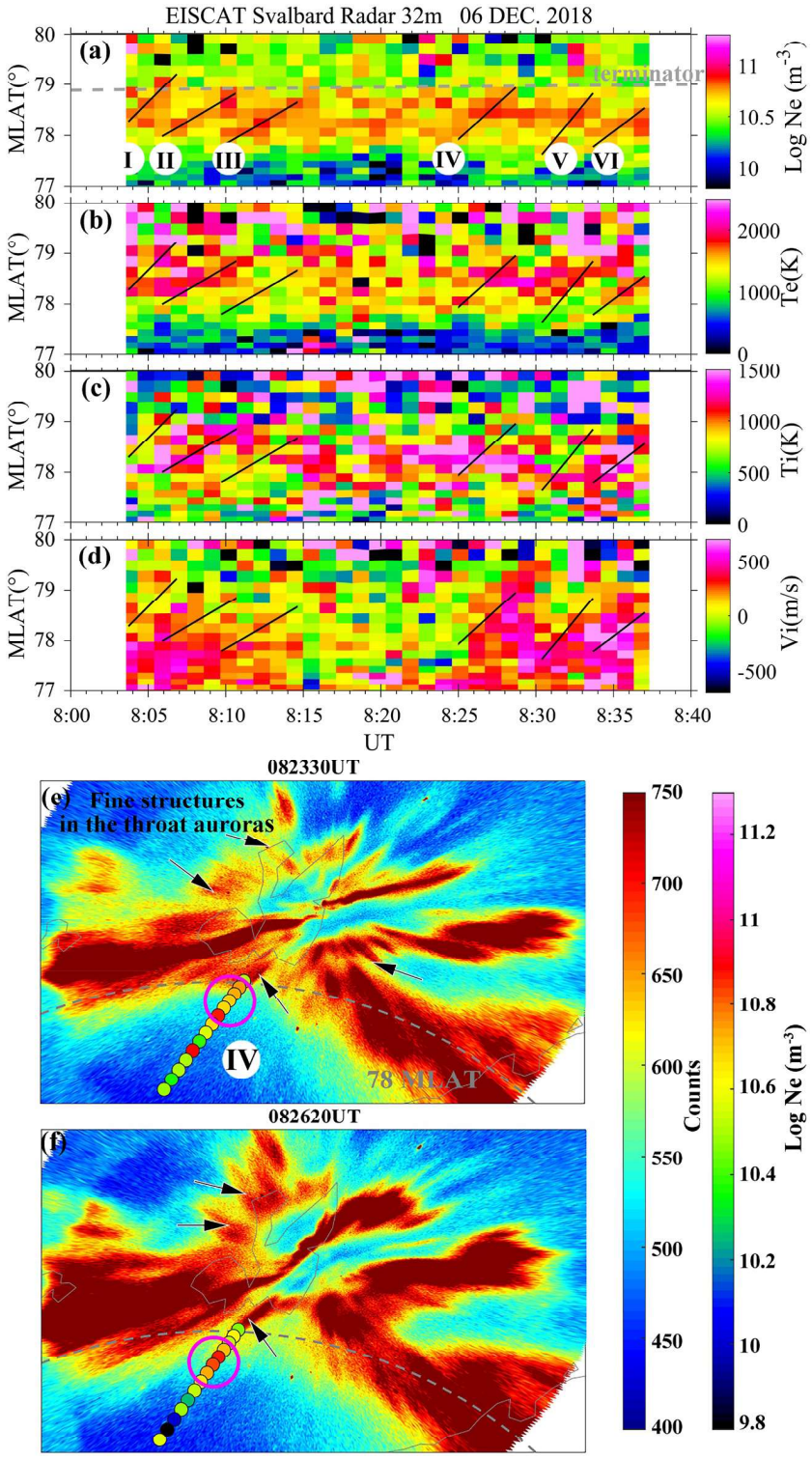

Figure 4. (a) Electron density, (b and c) ion and electron temperatures, and (d) ion line-of-sight velocity observed by the ESR 32 m. Positive velocities are away from the radar. The dashed gray line highlights the terminator location along the geomagnetic longitude of Longyearbyen (~111°E) at 300 km. (e and f) The 630.0 nm YRS ASI overlaid with ESR 32 m electron density observations plotted in magnetic local time-magnetic latitude coordinates at 082330 and 082620 UT. The black arrows with white borders highlight some fine-structures in the throat auroras. The magenta circles highlight patch "IV."

particle precipitation from ongoing reconnection will introduce additional ionization and a heat source (Walker et al., 1999). Thus, the patches, which are created from throat auroras, may also be a mix of cold and hot patches that experience Joule heating as they are transported (Lorentzen et al., 2010), which is observed by the ESR 32 m (Figure 4c). Moreover, the patches move anti-sunward along with convection streamlines due to the $E \times B$ plasma drift. This is supported by the electron density enhancement observed by the Swarm A and C. In order to clarify whether anti-sunward transport of dense plasma plays a major role, we calculated the plasma $E \times B$ drift velocity using the equation:

$$\overrightarrow{V_D} = \frac{\overrightarrow{E} \times \overrightarrow{B}}{B^2}$$

B is the magnetic field strength obtained through the International Geomagnetic Reference Field (IGRF) model, which is about 50,000 nT at 79° MLAT and 250 km. $E = \frac{\emptyset_D}{L}$ (assuming a uniform electric field near the throat region) is the electric field strength, where L is the ionospheric footprint length (~500 km) of the dayside magnetopause reconnection X-line. E is around 0.01 V/m before 0820 UT and then changes to 0.022 V/m. Therefore, the $E \times$ B plasma drift velocity changes from 200 m/s to 440 m/s, which is consistent with the ESR 32m observation (e.g., $V_{\text{patch'III'}} = 80$ km/300s = 267 m/s, $V_{\text{patch'IV'}} = 100$ km/200s = 500 m/s). This supports anti-sunward transport ($E \times B$ drift) as a significant contributor to the patches' evolution.

Note that the background plasma density was quite low in 2018 (solar minimum). The observed patches had F-region electron densities of less than 10^{11} m^{-3} (Figures 2g and 4a), which is more than one order of magnitude smaller than during solar maximum. The lower patch densities are a result of both generally lower electron densities at subauroral latitudes during solar minimum (less solar EUV ionization) and less ionization from particle precipitation in the dayside aurora. So, we only classify the patches based on their electron and ion temperatures.

5. Conclusion

A multi-instrument campaign was organized in the polar ionosphere, with three YRS ASIs, ESR, DMSP, and Swarm observations. We have used this data to analyze the formation of throat auroras and polar cap patches on 6 December 2018, and found evidence that the two were linked together. The throat auroras moved poleward from lower to higher latitudes and then faded. The patches then appeared just poleward of the faded throat auroras and continued to move poleward at about the same speed as the throat auroras. The throat auroras were associated with soft-electron precipitation, which was indicated by the red line emission intensity increasing with dayside magnetopause reconnection. The high-density plasma from subauroral latitudes moved poleward along with fine structures in the throat auroras in the form of patches, being transported by the anti-sunward $E \times B$ plasma drift. This paper links throat auroras and polar cap patches, where magnetic reconnection events associated with throat auroras can serve as a formation mechanism for polar cap patches for radial IMF (B_x-dominated) conditions.

Acknowledgments
The work in China was supported by the National Natural Science Foundation of China (Grants 42120104003, 42030101, 41874170, 41831072 and 42204164), the Stable-Support Scientific Project of China Research Institute of Radiowave Propagation (Grant A132101W02), the Chinese Meridian Project, the China Postdoctoral Science Foundation (Grant 2021M701974), the International Partnership Program of Chinese Academy of Sciences (Grant 183311KYSB20200003), Shandong Provincial Natural Science Foundation (Grant ZR2022QD077) and China Scholarship Council (Grant 202206220115). The work in Norway is supported by the Research Council of Norway Grant 223252. This research was supported by the International Space Science Institute (ISSI) in Bern and Beijing, through ISSI International Team project #511 (Multi-Scale Magnetosphere-Ionosphere-Thermosphere Interaction).

Data Availability Statement

The Johns Hopkins University Applied Physics Laboratory has provided the DMSP F17/SSUSI data (https://ssusi.jhuapl.edu/data_availability?spc=f17&type=edr-aur). The ESA has provided the Swarm satellites data (https://earth.esa.int/eogateway/catalog). The NASA OMNI database (http://omniweb.gsfc.nasa.gov) provides the IMF data. The of YRS ASIs and DMSP SSJ/5 data (from CEDAR Madrigal database) are provided in https://doi.org/10.5281/zenodo.7638354. The SuperDARN data is obtained from http://vt.superdarn.org/tiki-index.php?page=ASCIIData.

References

Buchert, S., Zangerl, F., Sust, M., André, M., Eriksson, A., Wahlund, J., & Opgenoorth, H. (2015). SWARM observations of equatorial electron densities and topside GPS track losses. *Geophysical Research Letters*, *42*(7), 2088–2092. https://doi.org/10.1002/2015GL063121

Carlson, H. C. (2012). Sharpening our thinking about polar cap ionospheric patch morphology, research, and mitigation techniques. *Radio Science*, *47*(4), RS0L21. https://doi.org/10.1029/2011RS004946

Carlson, H. C., Oksavik, K., Moen, J., & Pedersen, T. (2004). Ionospheric patch formation: Direct measurements of the origin of a polar cap patch. *Geophysical Research Letters*, *31*(8), L08806. https://doi.org/10.1029/2003GL018166

Coley, W. R., & Heelis, R. A. (1995). Adaptive identification and characterization of polar ionization patches. *Journal of Geophysical Research*, *100*(A12), 23819–23827. https://doi.org/10.1029/95JA02700

Han, D. S. (2019). Ionospheric polarization electric field guiding magnetopause reconnection: A conceptual model of throat aurora. *Science China Earth Sciences*, *62*(12), 2099–2105. https://doi.org/10.1007/s11430-019-9358-8

Han, D. S., Chen, X., Liu, J., Qiu, Q., Keika, K., Hu, Z., et al. (2015). An extensive survey of dayside diffuse aurora based on optical observations at Yellow River Station. *Journal of Geophysical Research: Space Physics*, *120*(9), 7447–7465. https://doi.org/10.1002/2015JA021699

Han, D.-S., Hietala, H., Chen, X.-C., Nishimura, Y., Lyons, L. R., Liu, J.-J., et al. (2017). Observational properties of dayside throat aurora and implications on the possible generation mechanisms. *Journal of Geophysical Research: Space Physics*, *122*(2), 1853–1870. https://doi.org/10.1002/2016JA023394

Han, D. S., Nishimura, Y., Lyons, L. R., Hu, H. Q., & Yang, H. G. (2016). Throat aurora: The ionospheric signature of magnetosheath particles penetrating into the magnetosphere. *Geophysical Research Letters*, *43*(5), 1819–1827. https://doi.org/10.1002/2016GL068181

Han, D.-S., Xu, T., Jin, Y., Oksavik, K., Chen, X.-C., Liu, J.-J., et al. (2019). Observational evidence for throat aurora being associated with magnetopause reconnection. *Geophysical Research Letters*, *46*(13), 7113–7120. https://doi.org/10.1029/2019GL083593

Hardy, D. A., Holeman, E. G., Burke, W. J., Gentile, L. C., & Bounar, K. H. (2008). Probability distributions of electron precipitation at high magnetic latitudes. *Journal of Geophysical Research*, *113*(A6), A06305. https://doi.org/10.1029/2007JA012746

Hosokawa, K., Taguchi, S., & Ogawa, Y. (2016). Periodic creation of polar cap patches from auroral transients in the cusp. *Journal of Geophysical Research: Space Physics*, *121*(6), 5639–5652. https://doi.org/10.1002/2015JA022221

Hosokawa, K., Zou, Y., & Nishimura, Y. (2019). Airglow patches in the polar cap region: A review. *Space Science Reviews*, *215*(8), 53. https://doi.org/10.1007/s11214-019-0616-8

Hu, Z.-J., Yang, H., Huang, D., Araki, T., Sato, N., Taguchi, M., et al. (2009). Synoptic distribution of dayside aurora: Multiple-wavelength all-sky observation at Yellow River Station in Ny-Ålesund, Svalbard. *Journal of Atmospheric and Solar-Terrestrial Physics*, *71*(8–9), 794–804. https://doi.org/10.1016/j.jastp.2009.02.010

Hu, Z.-J., Yang, Q.-J., Liang, J.-M., Hu, H.-Q., Zhang, B.-C., & Yang, H.-G. (2017). Variation and modeling of ultraviolet auroral oval boundaries associated with interplanetary and geomagnetic parameters. *Space Weather*, *15*(4), 606–622. https://doi.org/10.1002/2016SW001530

Jin, Y.-Y., Xing, Z.-Y., Zhang, Q.-H., Wang, Y., & Ma, Y.-Z. (2018). Polar cap patches observed by the EISCAT Svalbard radar: A statistical study of its dependence on the solar wind and IMF conditions. *Journal of Atmospheric and Solar-Terrestrial Physics*, *192*, 104768. https://doi.org/10.1016/j.jastp.2018.01.011

Knight, H. K., Strickland, D. J., Hecht, J. H., Straus, P. R., Morrison, D., Paxton, L. J., & Evans, D. S. (2008). Evidence for significantly greater N_2 Lyman-Birge-Hopfield emission efficiencies in proton versus electron aurora based on analysis of coincident DMSP SSUSI and SSJ/5 data. *Journal of Geophysical Research*, *113*(A4), A04305. https://doi.org/10.1029/2007JA012728

Liou, K., Newell, P. T., Meng, C.-I., Brittnacher, M., & Parks, G. (1998). Characteristics of the solar wind controlled auroral emissions. *Journal of Geophysical Research*, *103*(A8), 17543–17557. https://doi.org/10.1029/98JA01388

Lockwood, M., & Carlson, H. C. (1992). Production of polar cap electron density patches by transient magnetopause reconnection. *Geophysical Research Letters*, *19*(17), 1731–1734. https://doi.org/10.1029/92GL01993

Lorentzen, D. A., Moen, J., Oksavik, K., Sigernes, F., Saito, Y., & Johnsen, M. G. (2010). In situ measurement of a newly created polar cap patch. *Journal of Geophysical Research*, *115*(A12), A12323. https://doi.org/10.1029/2010JA015710

Ma, Y.-Z., Zhang, Q.-H., Xing, Z.-Y., Heelis, R. A., Oksavik, K., & Wang, Y. (2018). The ion/electron temperature characteristics of polar cap classical and hot patches and their influence on ion upflow. *Geophysical Research Letters*, *45*(6), 8072–8080. https://doi.org/10.1029/2018GL079099

Milan, S., Gosling, J., & Hubert, B. (2012). Relationship between interplanetary parameters and the magnetopause reconnection rate quantified from observations of the expanding polar cap. *Journal of Geophysical Research*, *117*(A3), A03226. https://doi.org/10.1029/2011JA017082

Moen, J., Oksavik, K., & Carlson, H. C. (2004). On the relationship between ion upflow events and cusp auroral transients. *Geophysical Research Letters*, *31*(11), L11808. https://doi.org/10.1029/2004GL020129

Nishimura, Y., Lyons, L. R., Zou, Y., Oksavik, K., Moen, J. I., Clausen, L. B., et al. (2014). Day-night coupling by a localized flow channel visualized by polar cap patch propagation. *Geophysical Research Letters*, *41*(11), 3701–3709. https://doi.org/10.1002/2014GL060301

Ogawa, Y., Fujii, R., Buchert, S. C., Nozawa, S., & Ohtani, S. (2003). Simultaneous EISCAT Svalbard radar and DMSP observations of ion upflow in the dayside polar ionosphere. *Journal of Geophysical Research*, *108*(A3), 1101. https://doi.org/10.1029/2002JA009590

Paxton, L. J., Meng, C. I., Fountain, G. H., Ogorzalek, B. S., Darlington, E. H., Goldstein, J., et al. (1992). Special sensor UV spectrographic imager (SSUSI): An instrument description. *Instrumentation for Planetary and Terrestrial Atmospheric Remote Sensing*, *1745*, 2–15.

Rodriguez, J. V., Carlson, H. C., & Heelis, R. A. (2012). Auroral forms that extend equatorward from the persistent midday aurora during geomagnetically quiet periods. *Journal of Atmospheric and Solar-Terrestrial Physics*, *86*, 6–24. https://doi.org/10.1016/j.jastp.2012.06.001

Southwood, D. J. (1987). The ionospheric signature of flux transfer events. *Journal of Geophysical Research*, *92*(A4), 3207. https://doi.org/10.1029/JA092iA04p03207

Walker, I. K., Moen, J., Kersley, L., & Lorentzen, D. A. (1999). On the possible role of cusp/cleft precipitation in the formation of polar-cap patches. *Annales Geophysicae*, *17*(10), 1298–1305. https://doi.org/10.1007/s00585-999-1298-4

Zhang, D., Zhang, Q.-H., Ma, Y.-Z., Oksavik, K., Lyons, L. R., Xing, Z.-Y., et al. (2022). The dependence of cold and hot patches on local plasma transport and particle precipitation in Northern Hemisphere winter. *Geophysical Research Letters*, *49*(12), e2022GL098671. https://doi.org/10.1029/2022GL098671

Zhang, D., Zhang, Q.-H., Ma, Y.-Z., Oksavik, K., Lyons, L. R., Zhang, Y.-L., et al. (2021). Solar and geomagnetic activity impact on occurrence and spatial size of cold and hot polar cap patches. *Geophysical Research Letters*, *48*(18), e2021GL094526. https://doi.org/10.1029/2021GL094526

Zhang, Q.-H., Ma, Y.-Z., Jayachandran, P. T., Moen, J., Lockwood, M., Zhang, Y.-L., et al. (2017). Polar cap hot patches: Enhanced density structures different from the classical patches in the ionosphere. *Geophysical Research Letters*, *44*(16), 8159–8167. https://doi.org/10.1002/2017GL073439

Zhang, Q.-H., Xing, Z.-Y., Wang, Y., & Ma, Y.-Z. (2020). Formation and evolution of polar cap ionospheric patches and their associated upflows and scintillations: A review. In Q. G. Zong, P. Escoubet, D. Sibeck, G. Le, & H. Zhang (Eds.), *Dayside magnetosphere interaction* (pp. 286–302). John Wiley & Sons, Inc. https://doi.org/10.1002/9781119509592.ch16

Zhang, Q. H., Zhang, B. C., Hu, H. Q., Moen, J., Lockwood, M., McCrea, I. W., et al. (2013). Polar cap patch segmentation of the tongue of ionization in the morning convection cell. *Geophysical Research Letters*, *40*(12), 2918–2922. https://doi.org/10.1002/grl.50616

Zhang, Q.-H., Zhang, B.-C., Liu, R.-Y., Dunlop, M. W., Lockwood, M., Moen, J., et al. (2011). On the importance of IMF |BY| on polar cap patch formation. *Journal of Geophysical Research*, *116*(A5), A05308. https://doi.org/10.1029/2010JA016287